

www.acsami.org Research Article

Chemically Edge-Carboxylated Graphene Enhances the Thermal Conductivity of Polyetherimide—Graphene Nanocomposites

Fatema Tarannum, Rajmohan Muthaiah, Swapneel Danayat, Kayla Foley, Roshan S. Annam, Keisha B. Walters, and Jivtesh Garg*



Cite This: ACS Appl. Mater. Interfaces 2022, 14, 14753–14763



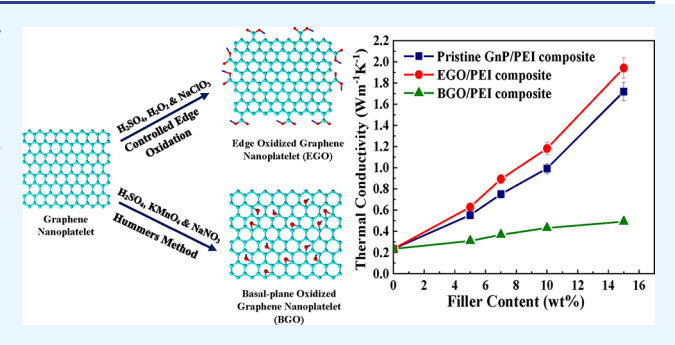
ACCESS

III Metrics & More

Article Recommendations

s Supporting Information

ABSTRACT: In this work, we demonstrate that edge oxidation of graphene can enable larger enhancement in thermal conductivity (k) of graphene nanoplatelet (GnP)/polyetherimide (PEI) composites relative to oxidation of the basal plane of graphene. Edge oxidation offers the advantage of leaving the basal plane of graphene intact, preserving its high in-plane thermal conductivity ($k_{\rm in} > 2000~{\rm W~m^{-1}~K^{-1}}$), while, simultaneously, the oxygen groups introduced on the graphene edge enhance interfacial thermal conductance through hydrogen bonding with oxygen groups of PEI, enhancing the overall polymer composite thermal conductivity. Edge oxidation is achieved in this work by oxidizing graphene in the



presence of sodium chlorate and hydrogen peroxide, thereby introducing an excess of carboxyl groups on the edge of graphene. Basal plane oxidation of graphene, on the other hand, is achieved through the Hummers method, which distorts the $\rm sp^2$ carbon—carbon network of graphene, dramatically lowering its intrinsic thermal conductivity, causing the BGO/PEI (BGO = basal-plane oxidized graphene or basal-plane-functionalized graphene oxide) composite's k value to be even lower than pristine GnP/PEI composite's k value. The resulting thermal conductivity of the EGO/PEI (EGO = edge-oxidized graphene or edge-functionalized graphene oxide) composite is found to be enhanced by 18%, whereas that of the BGO/PEI composite is diminished by 57%, with respect to the pristine GnP/PEI composite with 10 wt % GnP content. Two-dimensional Raman mapping of GnPs is used to confirm and distinguish the location of oxygen functional groups on graphene. The superior effect of edge bonding presented in this work can lead to fundamentally novel pathways for achieving high thermal conductivity polymer composites.

KEYWORDS: graphene, oxidation, polymer nanocomposites, thermal conductivity, interface, edge, basal plane

1. INTRODUCTION

Thermal management has become a challenging issue in modern electronics due to continuous miniaturization of electronic components which results in increasing heat fluxes. To improve the efficiency and reliability of electronic systems, heat needs to be dissipated efficiently. In terms of material selection, polymers offer several advantages over metals such as a low cost, corrosion resistance, ease of moldability, and a lower weight. High thermal conductivity polymer materials can improve thermal management in a wide range of applications, such as water desalination,² automotive control units,³ batteries, solar panels, supercapacitors, electronic packaging, and electronic cooling. A key approach to enhance the thermal conductivity of polymers is addition of high thermal conductivity fillers such as graphene ($k > 2000 \text{ W m}^{-1} \text{ K}^{-19,10}$). Different approaches have been used to enhance the composite k value through graphene, such as the synergistic effect with multiple fillers 11 and alignment of graphene. 12,13 The success of these approaches is, however, limited by the large interface thermal resistance between graphene and the polymer in the range of 10^{-8} to 10^{-7} m² K W^{-113,14} due to mismatch of phonons (lattice vibrations) between the two. To decrease the thermal interface resistance, graphene is chemically functionalized by groups that are compatible with the surrounding polymer. ^{15,16} Covalent functionalization and non-covalent functionalization of graphene can lead to higher interfacial thermal conductance. Two orders of magnitude increase in interface thermal conductance and 156% enhancement functionalization of polymer chains on graphene. Recent work demonstrated that multilayer graphene is more efficient in enhancing thermal conductivity than single-layer graphene. For such multilayer graphene, it is critically important to understand the optimal location of functional groups (such as the edge or basal plane of graphene, Figure 1a—d), which can lead to highest

Received: December 31, 2021 Accepted: March 3, 2022 Published: March 15, 2022





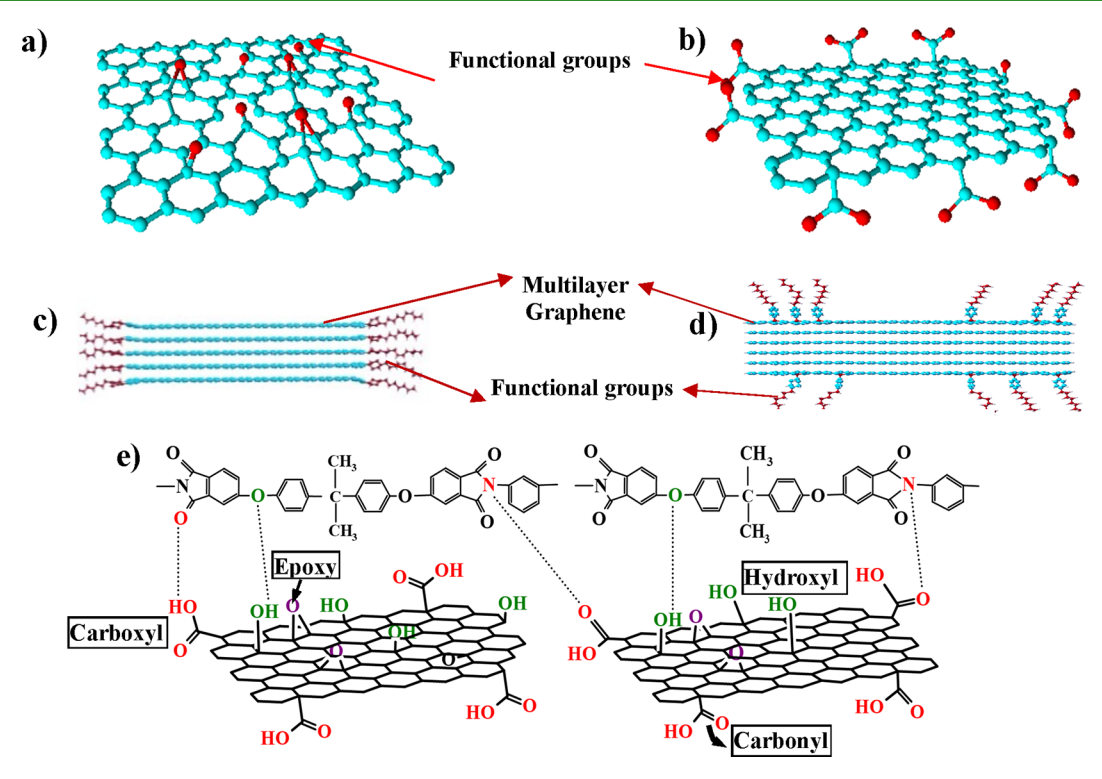


Figure 1. Atomic structure of (a) functionalized single graphene sheet with basal-plane functional groups and (b) functionalized single graphene sheet with edge functional groups. Atomic structures of (c) multilayer edge-functionalized graphene and (d) multilayer basal-plane-functionalized graphene. (e) Interactions between graphene oxide and PEI.

composite thermal conductivity. In this work, we demonstrate that functionalization on the edges (Figure 1b,c) can lead to significantly higher effective polymer thermal conductivity compared to functionalization on the basal plane (Figure 1a,d). The functionalization scheme used in this work is oxidation of graphene because oxygen groups on graphene can interact with oxygen groups in polyetherimide (PEI) through hydrogen bonding (Figure 1e). Edge oxidation is achieved in this work using a recently introduced chemical pathway, by oxidizing graphene in the presence of sodium chlorate and hydrogen peroxide to introduce excess of carboxyl moieties.²⁰ Oxidation of the basal plane is achieved through the Hummers method.²¹

Several computational and experimental studies have reported the enhancement of thermal conductivity through functionalization. Theoretical studies on polymer-grafted graphene (performed by Wang et al.) showed 2-fold lower interfacial thermal resistance through attachment of functional groups.²² Using molecular dynamics (MD) simulations, Konatham et al.²³ demonstrated almost 50% reduction in the interfacial thermal resistance between functionalized graphene and octane. Lin and Buehler¹⁶ showed, using MD simulations, a 22% increase in interface thermal conductance through use of alkyl-pyrene functional groups. Ganguli et al.24 showed that silane-functionalized graphene improved the thermal conductivity of a graphene/epoxy composite by 50% compared to a pristine graphene composite with 8 wt % graphene content. A pyrene-end poly(glycidyl methacrylate)-functionalized graphene/epoxy composite was found to yield ~184% enhancement in thermal conductivity over pure epoxy.²⁵ A comparison between edge and basal plane functionalization has also been carried out for several applications. Yang et al.²⁶ compared the role of edge and basal plane functionalization in modifying the interfacial tension between graphene and liquids. Mungse et

al.²⁷ studied the lubrication potential of basal plane-alkylated graphene nanosheets. In another study, the effect of an interconnected three-dimensional network structure of the edge- or basal plane-modified graphene oxide on electrical conductivity²⁸ was examined. Xiang et al.²⁹ compared edge versus basal plane functionalization of graphene for energy conversion and energy storage applications. There is, however, a lack of detailed understanding of the relative effectiveness of edge versus basal plane functionalization in enhancing the thermal conductivity of polymer—graphene nanocomposites.

The advantage of edge oxidation can be understood by observing that oxidation of the basal plane through the Hummers method²¹ distorts the planar sp²-sp² carbon network of the basal plane by requiring a transition to tetrahedral sp³ hybridization needed to accommodate the extra bond for oxidation (Figure 1a). These sites of distortion act as phonon scatterers, dramatically lowering the intrinsic thermal conductivity of graphene. In general, a subsequent reduction reaction is required to partially restore the sp² carbon—carbon network before graphene can be used to enhance the thermal conductivity of composites. The defective structure of basal plane-oxidized graphene (BGO) has been studied through Xray diffraction (XRD), scanning tunneling microscopy, and Raman scattering. 30,31 The oxidation-related defects are found to be mainly due to the presence of hydroxyl (-OH) and epoxy (C-O-C) functional groups on the basal plane of graphene.30 Bagri et al. also studied the defective state of GO and indicated the presence of hydroxyl and epoxy groups on the basal plane as the main defect sites.³² We later show the presence of these functional groups in BGO through Fourier transform infrared (FTIR) spectroscopy, thermogravimetric analysis (TGA) and X-ray photoelectron spectroscopy (XPS) in Sections 3.5, 3.6, and 3.7, respectively. Reduction in thermal

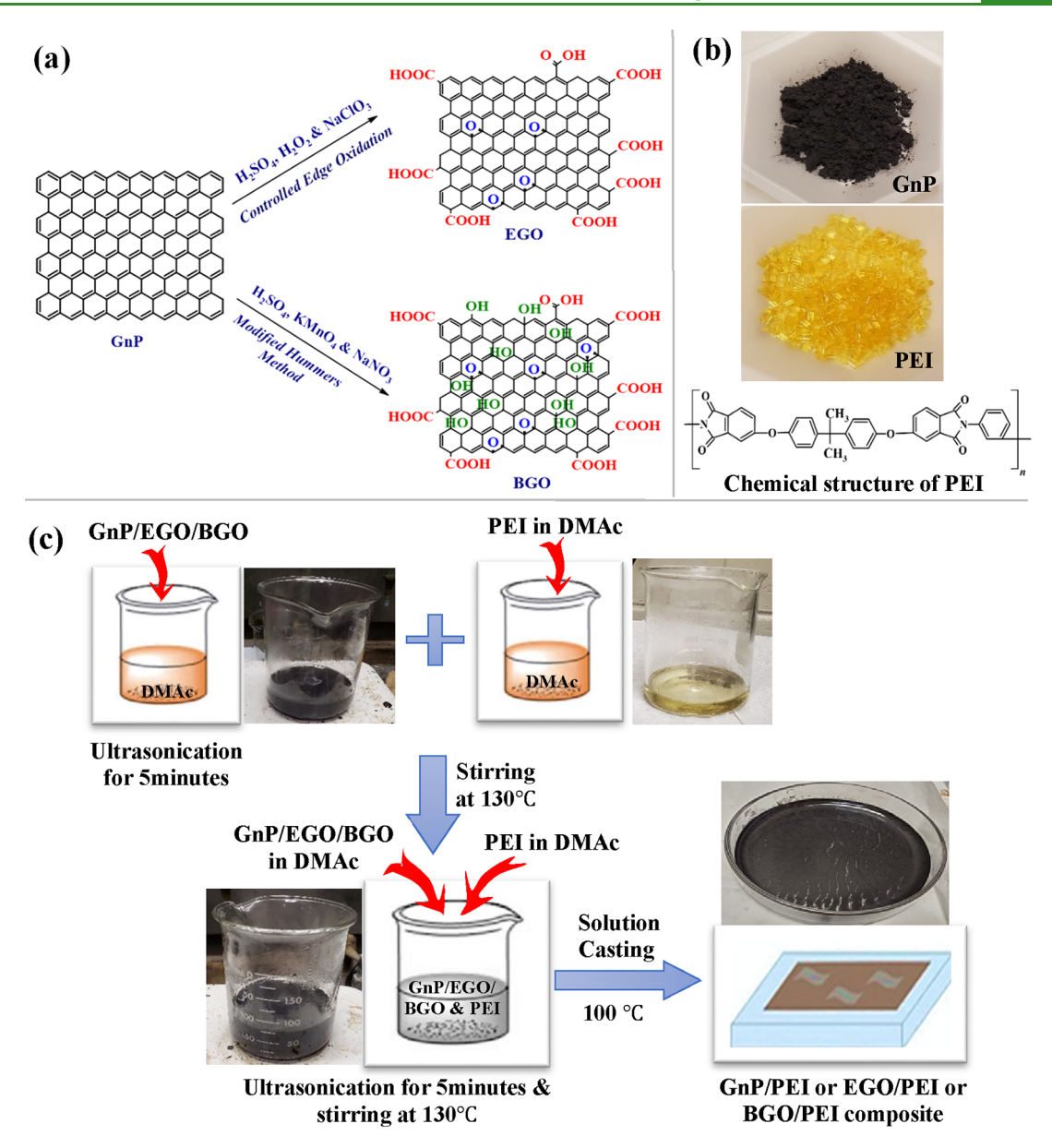


Figure 2. (a) Schematic structure of GnP, EGO, and BGO (carboxyl and carbonyl groups: -COOH/-C=O; epoxy group: C-O-C; and hydroxyl group: -OH), (b) images of the GnP nanopowder, PEI pellets, and the chemical structure of PEI, and (c) scheme of polymer–graphene composite preparation; DMAc—N,N-dimethylacetamide.

conductivity through such functionalization of the basal plane has been well studied computationally. While the intrinsic thermal conductivity of graphene is ~2000 W m⁻¹ K⁻¹, Fugallo et al. used first-principles computations to report that this value dropped by a factor of 2 in hydrogenated graphene and by 1 order of magnitude in fluorogenated graphene.³³ Mu et al.³⁴ used molecular dynamics simulations to predict a dramatic decrease in the thermal conductivity of BGO. An oxygen coverage of mere 5% was shown to reduce the k value of BGO dramatically by 90% and a coverage of 20% lowered it further to $\sim 8.8 \text{ W m}^{-1} \text{ K}^{-1}$, even lower than the amorphous limit. Shenogin et al.³⁵ similarly used MD simulations to show a decrease in k of carbon nanomaterials through functionalization. The much lower thermal conductivity of basal planefunctionalized graphene limits its effectiveness in enhancing the thermal conductivity of the polymer composite and can even result in a decrease in composite thermal conductivity relative to the case of pristine graphene. A reduction reaction

with different reactants³⁶ or simultaneous amination³⁷ is used to partially restore the thermal conductivity of graphene. 15.8 wt % thermally reduced RGO/epoxy composites (prepared using a modified Hummers method, followed by a two-step reduction reaction) yielded a k value of 1.27 W m⁻¹ K⁻¹ (relative to 0.275 W m⁻¹ K⁻¹ for pure epoxy).³⁸ An aminefunctionalized GO/PEI composite exhibited thermal conductivity values up to 0.33 W m⁻¹ K⁻¹ at 3 wt % phenyl aminated graphene-oxide filler concentration³⁹ (showing an enhancement of 43% relative to the pure PEI thermal conductivity of 0.23 W m⁻¹ K⁻¹). Bernal et al. prepared a graphene nanopaper from phenol-functionalized graphene and linked this phenol-functionalized graphene with dianiline and directly measured a k value of 0.672 W m⁻¹ K⁻¹, demonstrating 190% enhancement with respect to the pristine GnP nanopaper.40

Edge oxidation of graphene offers the advantage of leaving the basal plane intact (Figure 1b), preserving its ultrahigh thermal conductivity (\sim 2000 W m⁻¹ K⁻¹).¹⁴ Using MD simulations, the thermal conductivity of edge-functionalized graphene has been shown to be within 90% of the pristine graphene value.⁴¹ Simultaneously, hydrogen bonding interaction between oxygen groups of graphene (on edge) and PEI enhances the interfacial thermal conductance between graphene and PEI. The preserved high thermal conductivity of graphene coupled with superior interfacial thermal conductance of a polymer can lead to superior enhancement in thermal conductivity of a polymer composite through edge oxidation, compared to the case of BGO.

In our recent computational work,⁴¹ we also demonstrated other advantages of edge functionalization for enhancement of composite thermal conductivity. We showed that edge bonding couples a polymer to the high in-plane ($k_{\rm in} > 2000 \ {\rm W m}^{-1}$ K⁻¹)⁹ thermal conduction pathway of all graphene sheets within an nP (Figure 1c), thus establishing a very efficient thermal conduction path through the composite. Basal plane bonding, on the other hand, primarily couples functional groups only to the outermost surface layers of the GnP (Figure 1d). The weak van der Waals' coupling of outer layers with inner layers renders the inner layers of the GnP to be less efficient in conducting heat due to the poor through-thickness thermal conductivity of graphite $(\sim 10 \text{ W m}^{-1} \text{ K}^{-1})^{13,42}$ (Figure 1d). We further demonstrated that edge bonding leads to weak damping of vibrations within the graphene sheets, while for basal plane bonding, the coupling of the entire basal plane with an embedding polymer was found to strongly dampen vibrations, further promoting the advantage of edge bonding. Finally, we demonstrated using ab initio atomistic Green's function computations⁴³ that interfacial thermal conductance at an individual junction between a functional group and graphene was higher, when the functional group was located on the edge, as opposed to on the basal plane of graphene. This higher interfacial conductance is explained in terms of higher transmission to in-plane phonons of graphene for the edge-bonding case.

The above computational results provide a comprehensive understanding of the advantage of edge bonding in enabling superior thermal conductivity enhancement of a composite. In this work, we demonstrate this advantage of edge bonding experimentally. Selective edge oxidation of graphene is obtained in this work by using the scheme outlined by Miao et al.²⁰ involving oxidizing graphene in the presence of sodium chlorate and hydrogen peroxide in sulfuric acid. Miao et al.²⁰ showed that such a scheme leads to excess carboxyl groups on the edge of oxidized graphene. We confirm the presence of excess carboxyl groups through the above oxidation scheme using FTIR and XPS analyses in Sections 3.5 and 3.7, respectively. Carboxyl groups are known to preferentially form on the edge of graphene, yielding edge-oxidized graphene (EGO). To experimentally show the edge localization of carboxyl groups, Yuge et al.44 stained carboxyl groups using a Pt-amine complex and found Pt-amine clusters to mainly exist at the edges of graphene sheets. Computations based on density functional theory also showed through geometric arguments that carboxyl groups are more likely to form on graphene edges. 45 This work is the first to report enhancement in thermal conductivity through the use of the chemical edge oxidation pathway discussed above. Basal plane oxidation was achieved by using the Hummers method²¹ by oxidizing graphene in the presence of sodium nitrate and potassium permanganate.

The preferential edge functionalization through Miao's scheme²⁰ is confirmed in this work through location-dependent two-dimensional (2D) Raman mapping of GnPs. Functionalized graphene is further characterized using XRD, XPS, TGA, FTIR spectroscopy, and scanning and transmission electron microscopy (SEM and TEM) to examine the physical and chemical differences between the pristine graphene, EGO, and BGO.

2. EXPERIMENTAL SECTION

2.1. Materials. GnPs used in this work have an average thickness of \sim 60 nm and a lateral size of \sim 7 μ m. The graphene nanopowder was purchased from Graphene Supermarket. Potassium permanganate (KMnO₄, 99%), sulfuric acid (H₂SO₄, 95–98%), hydrogen peroxide (H₂O₂, 30%), sodium chlorate (NaClO₃, 99%), sodium nitrate (NaNO₃), DMAc, hydrochloric acid (HCl, 35.0–37.0%), and PEI (PEI pellets, melt index: 18 g/10 min) were purchased from Sigma-Aldrich.

2.2. Synthesis of Edge-Functionalized Graphene Oxide. The synthesis of EGO was performed with a controlled oxidation reaction using NaClO₃, H₂SO₄, and H₂O₂ (Figure 2a) according to the approach outlined by Miao et al.²⁰ 80 mL of H₂SO₄ was cooled down to 0 °C temperature using an ice bath, and 1 gm of graphenenanopowder was dispersed into H₂SO₄ using bath sonication for 15 min. After dispersing graphene into H_2SO_4 , approximately 6 mL of 30% H₂O₂ solution was added to the mixture and stirred at 0 °C for a few minutes. Then, 4 gm of NaClO3 was added very slowly and carefully into this mixture for 2 h. This mixture was kept stirring at room temperature for 8 h. The reaction mixture was then poured into 500 mL of cold DI water. The mixture was centrifuged at 4000 rpm to separate the particles from acidic solution. The separated particles were then washed twice with 800 mL of HCl aqueous solution (HCl/ DI water = 1:9), followed by repeated filtration with ethanol, acetone, and DI water until the pH reached the neutral condition. The product was then kept in a vacuum oven at 60 °C for 24 h. These oxidized particles are edge oxidized graphene.

2.3. Synthesis of Basal-Plane-Functionalized Graphene Oxide. The Hummers method²¹ was used to prepare basal-plane-functionalized graphene oxide (Figure 2a). For this synthesis, 1 g of graphene nanopowder was added to the mixture of 46 mL of sulfuric acid and 1 g of NaNO₃. This reaction was stirred for 4 h at 0 °C in an ice-cold bath to get a homogeneous dispersion. 6 g of KMnO₄ was added very slowly into this mixture. To maintain the temperature at 0 °C, the addition of KMnO₄ was done for 1 h. Then, the reaction mixture was kept stirring at 35 °C. After 6 h, the reaction mixture was added to 92 mL of DI water at 95 °C and stirred for 15 min. In the last step, this mixture was mixed with 20% H₂O₂ aqueous solution. The final product was washed several times with HCl aqueous solution, ethanol, acetone, and DI water repeatedly to remove ions and impurities. The separated particles were dried in a vacuum oven at 60 °C for 24 h to obtain the basal-plane oxidized graphene.

2.4. Preparation of Pristine GnP/PEI, EGO/PEI, and BGO/PEI Composites. A solution casting method was used to prepare the composites, and the through-thickness thermal conductivity values of these samples were then measured and compared. Pristine 60 nm GnPs were dispersed into 20 mL DMAc for 30 min using a probe sonicator (Figure 2c). PEI pellets were separately dissolved into 50 mL DMAc at 130 °C for 1 h. Dispersed graphene solution was blended into dispersed polymer solution for 3 h at 130 °C. To disperse graphene into the polymer properly, graphene and polymer solutions were mixed together and ultrasonicated for 5 min. The homogenized solution was cast into a Petri dish and held at 100 °C for 24 h producing a graphene—PEI composite film. 7, 10, and 15 wt % GnP/PEI, EGO/PEI, and BGO/PEI composite films were prepared using the same procedure.

3. RESULTS AND DISCUSSION

3.1. Thermal Conductivity Data. Figure 3 presents the comparison of k values of GnP/PEI, EGO/PEI, and BGO/PEI

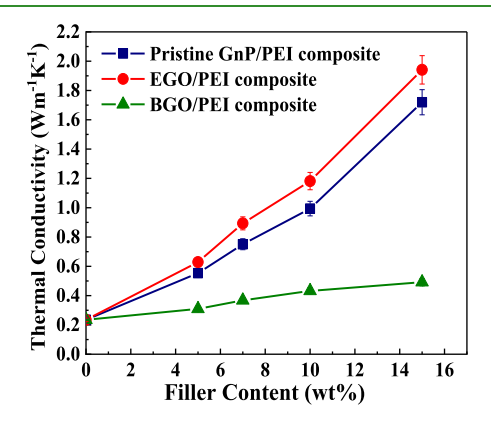


Figure 3. Through-thickness thermal conductivity of GnP/PEI, EGO/PEI and BGO/PEI composites with 5, 7, 10, and 15 wt % GnP content.

composites for different GnP filler loadings. The thermal conductivity (k) value of pure PEI is measured to be 0.23 W m⁻¹ K⁻¹ (in good agreement with the literature value⁴⁸), while thermal conductivity of the pristine graphene–PEI composite (shown by a blue curve in Figure 3) is measured to be 1.72 W m⁻¹ K⁻¹ for 15 wt % filler content. Figure 3 further shows that the highest thermal conductivity values are achieved through the use of EGO, clearly demonstrating the advantage of edge oxidation. Enhancements in the k value of 18 and 13% are achieved for the EGO/PEI composite relative to pristine GnP/PEI composite, resulting in high k values of 1.14 and 1.94 W m⁻¹ K⁻¹ for the EGO/PEI composite for 10 and 15 wt % graphene, respectively. The k value of 1.94 W m⁻¹ K⁻¹ achieved for the 15 wt % EGO/PEI composite represents a large enhancement of ~725% compared to that of pure PEI.

On the other hand, the k value of the BGO/PEI composite is found to be diminished relative to that of the pristine GnP/PEI composite. At 15 wt % composition, the k value of the BGO/PEI composite (0.48 W m⁻¹ K⁻¹) is lowered by almost

72 and 75% relative to those of pristine GnP/PEI and EGO/PEI composites, respectively. The BGO/PEI composite's k value is still found to be enhanced with respect to the pure PEI k value by $\sim 104\%$ at 15 wt % composition. This enhancement is, however, much smaller than the enhancement of 725% achieved for the EGO/PEI composite.

The lower k value of the BGO/PEI composite is due to the defects introduced by the Hummers method on the basal plane of GnP⁴⁹ (as discussed before), which dramatically lowers the intrinsic thermal conductivity of graphene. We later provide evidence (through the $I_{\rm D}/I_{\rm G}$ ratio obtained via Raman analysis in Section 3.3) for the presence of a much larger number of functional groups on the basal plane of graphene for BGO compared to pristine GnP and EGO. XRD analysis (presented in Section 3.4) further shows that these oxygen functional groups lead to an increase in the interlayer spacing of BGO to 0.717 nm (relative to the value of 0.336 nm for pristine GnP) indicating that the oxygen groups intercalate the spacing between the graphene layers within the GnP for BGO and attach to the basal planes of all graphene sheets constituting the GnP. Previous computations have shown that such BGO has a dramatically diminished k value compared to that of pristine graphene (by up to 90% lower for 5% coverage).³⁴ The significantly lower k value of BGO compared to that of pristine graphene causes the k value of the BGO/PEI composite to become even lower than that of the pristine GnP/PEI composite.

For edge bonding (EGO), however, we show through Raman analysis (in Section 3.3), a much smaller presence of functional groups on the basal plane of graphene. XRD analysis (discussed in Section 3.4) further shows that the interlayer spacing of EGO (0.337 nm) is very similar to that of pristine graphene (0.336 nm), providing more evidence for the presence of oxygen groups on the edges of graphene for EGO. XPS analysis (Section 3.7) further shows a stronger intensity of the C-C/C=C peak in EGO compared to that of BGO. These analyses point to superior structural integrity of the basal plane of graphene for EGO relative to BGO. Computational analysis reveals that k of such structurally preserved EGO can be close to the high intrinsic k of pristine graphene. Simultaneously, hydrogen bonding between oxygen

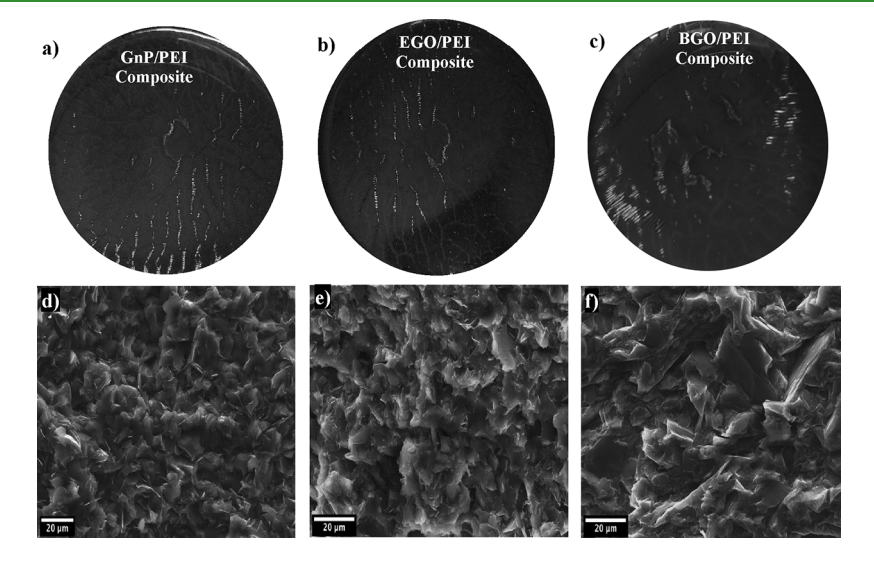


Figure 4. Images of composite films for (a) pristine GnP/PEI, (b) EGO/PEI, and (c) BGO/PEI and cross-sectional FE-ESEM images of 15 wt % composites for (d) pristine GnP/PEI, (e) EGO/PEI, and (f) BGO/PEI.

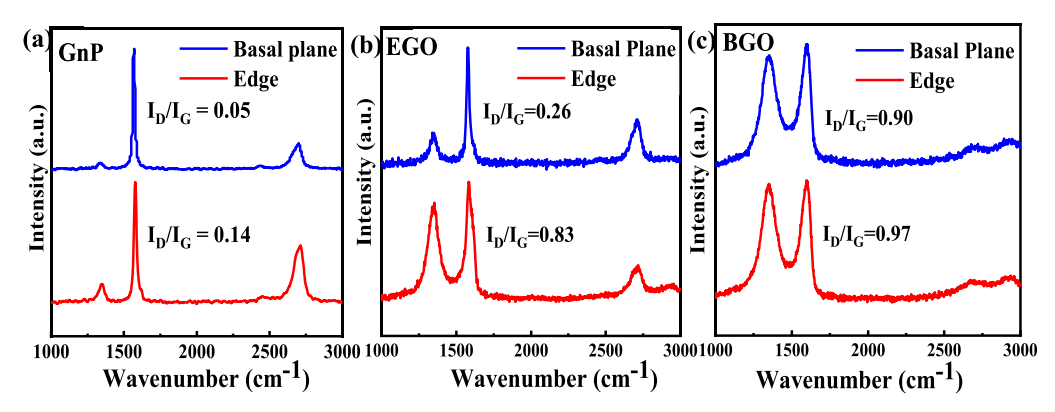


Figure 5. I_D/I_G ratio of the edge and basal plane area of (a) GnP, (b) EGO, and (c) BGO.

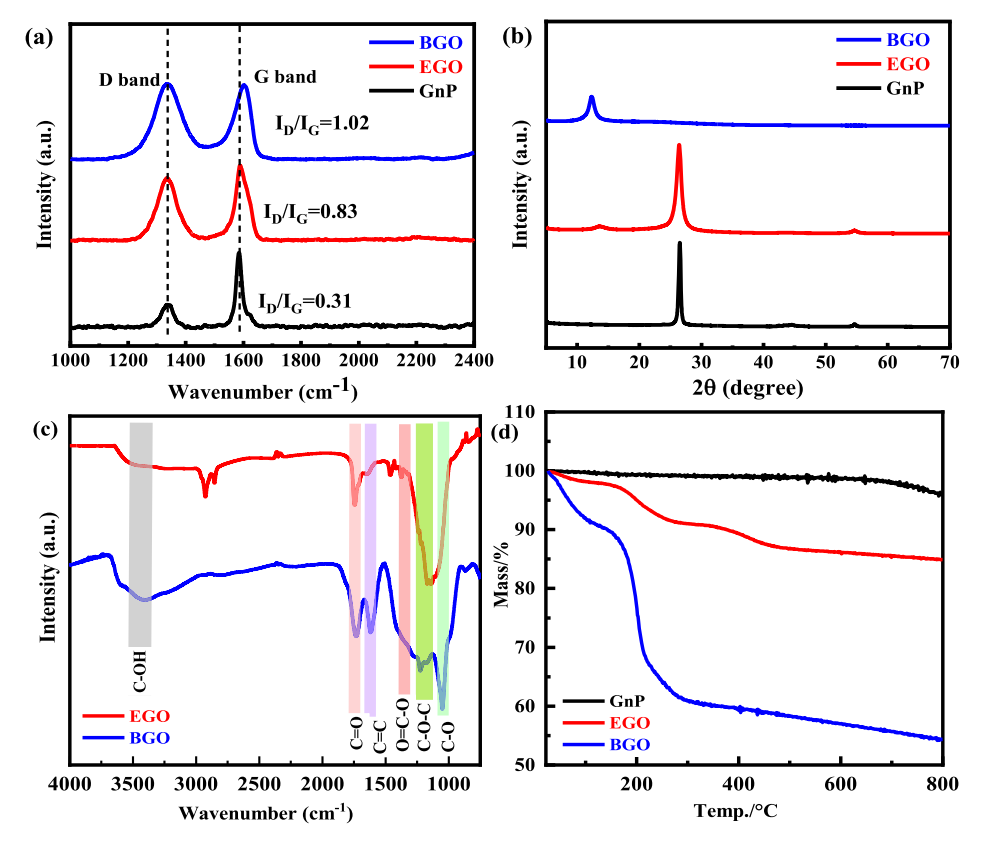


Figure 6. (a) Raman spectra, (b) full XRD spectra (c) FTIR, and (d) TGA spectra of GnP, EGO, and BGO.

groups of EGO and PEI enhances interfacial thermal conductance between the two. Significantly superior k of EGO (and close to the value of pristine graphene) compared to BGO, combined with improved interfacial thermal conductance between EGO and PEI (relative to the conductance between pristine GnP and PEI), causes the k of EGO/PEI to exceed those of both the pristine GnP/PEI and BGO/PEI composites (Figure 3). These results can enable new avenues to achieve higher thermal conductivity polymer/graphene nanocomposites. Below, we provide the details of dispersion of graphene in the prepared composite. We further provide understanding of differences in oxidation in EGO and BGO through detailed characterization.

3.2. Dispersion of GnPs within the Composite. Uniform dispersion of graphene in the polymer matrix is critical for achieving high thermal conductivity. In this work, we used DMAc to both dissolve PEI and disperse GnPs.

DMAc is a highly polar aprotic solvent and has a very strong dispersing power. This enables significantly lower aggregation compared to other solvents such as acetone or ethanol. Figure 4a-c shows that GnPs were uniformly dispersed in all three composites-pristine GnP/PEI, EGO/PEI, and BGO/PEI. While Figure 4a-c shows dispersion of graphene in bulk samples, we also performed cross-sectional FE-SEM analysis to study dispersion of graphene on a microscopic scale. These images are shown in Figure 4d-f for 15 wt % GnP/PEI, EGO/ PEI, and BGO/PEI composites. These images clearly indicate that pristine GnP, EGO, and BGO fillers are all similarly well dispersed into the polymer matrix even at a microscopic level. The similar uniform dispersion of graphene for all three cases (pristine, edge-oxidized, and basal-plane-oxidized) indicates that the advantage of edge bonding in enhancing k relative to pristine graphene can be attributed to superior interfacial thermal interaction with the surrounding PEI.

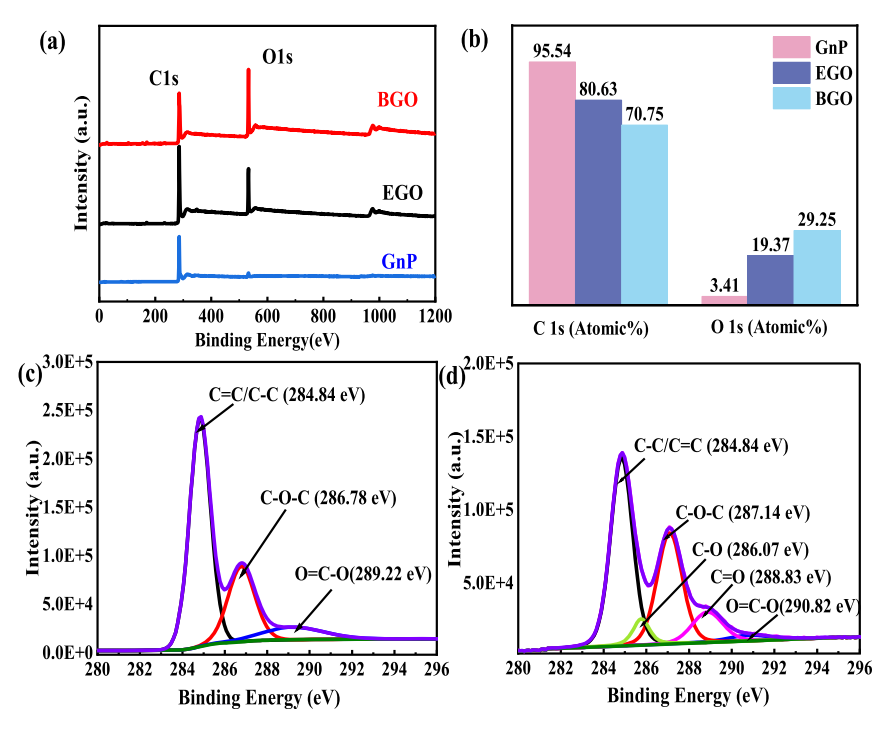


Figure 7. XPS data showing (a) survey spectra, (b) atomic percentage of C 1s and O 1s for GnP, EGO, and BGO, and the high resolution C 1s spectra for (c) EGO and (d) BGO.

3.3. Raman Characterization. To provide evidence for selective edge oxidation of graphene, 2D Raman mapping of EGO and BGO (Figure 5a-c) was performed. Raman spectroscopy characterizes the graphene's unique structure through two conventional peaks, one at $\sim 1586~\rm cm^{-1}$ and another one at $\sim 1345~\rm cm^{-1}$, attributed to the G band and D band, respectively.⁵⁰ The presence of the G band is related to the stretching mode of defect-free sp² carbon through the first order E2g scattering mode and the D band is induced by the disordered structure of sp³ hybridized carbon. I_D/I_G (the ratio of the intensity of the D band and G band), 52 thus provides an understanding of the structural disorder of the graphitic structure.

To examine and compare the $I_{\rm D}/I_{\rm G}$ ratio at the "edge" versus "basal plane" of both EGO and BGO, a DXR3 Raman microscope is used, and GnPs (pristine graphene/EGO/BGO) are transferred on a glass slide on top of a piece of doublesided tape to ensure that they do not move/drift during the Raman mapping. For treated/untreated graphene, one to two GnPs are selected for Raman area mapping. A snapshot of pristine GnPs captured during the 2D Raman mapping using a 100× objective is shown in Figure S1a. The red rectangle (as shown in Figure S1a) is the area (10 μ m × 4.2 μ m) selected for Raman mapping, with each red dot representing a spot for Raman spectral collection (total 147 points, with a step size of $0.5 \mu m$). The spectra were collected from points on the edge and basal plane area of GnPs separately to compare the $I_{\rm D}/I_{\rm G}$ ratio of the edge and basal planes for pristine GnP, EGO, and BGO. The process involved in 2D Raman mapping is presented in Supporting Information in Figure S1a-d.

These I_D/I_G ratios for the central area and edge are compared in Figure 5a-c for pristine GnP, EGO, and BGO. The I_D/I_G ratio increases more dramatically on edges (from 0.14 for pristine graphene to 0.83 for EGO) relative to the basal plane (from 0.05 for the pristine graphene to 0.26 for EGO) for EGO. This much larger increase of the I_D/I_G ratio on edges suggests that selective edge oxidation has taken place at the edges of EGO. However, for BGO, an increase in the I_D / $I_{\rm C}$ ratio on the basal plane is more significant (from 0.05 for pristinegraphene to 0.90 for BGO), suggesting basal plane oxidation for BGO.

The higher I_D/I_G ratio on the central area of BGO (0.90) compared to EGO (0.25) indicates a greater number of functional groups on the central area of BGO relative to EGO; these functional groups distort the basal plane of graphene in BGO, 26,53 causing a reduction in its thermal conductivity which in turn decreases the overall thermal conductivity of the BGO/PEI composite (Figure 5c). Overall, the I_D/I_C ratio (for the entire GnP) of EGO (0.83) is also significantly lower than that of BGO (1.02), indicating overall less structural damage in EGO compared to BGO (Figure 6a). More details of Raman analysis are presented in the Supporting Information (Table S1).

3.4. Effect of Functionalization on Interlayer Spacing through XRD Analysis. To further provide evidence for distortion of the graphitic structure in BGO, we performed XRD analysis to understand the interlayer spacing for the two different oxidation schemes. The interlayer spacing is measured from Bragg's law54 by using

$$n\lambda = 2d\sin\theta\tag{1}$$

where λ is the X-ray wavelength (0.15404 nm) and θ is the diffraction angle (radians). The XRD diffraction pattern of pristine GnP shows a sharp reflection peak (002) at 2θ = 26.5°55 (Figure 6b), pointing to an interlayer spacing (d) of 0.336 nm (computed from eq 2) for pristine GnP. For the GnPs of EGO, the diffraction peak is still sharp and intense at the same location $(2\theta = 26.4^{\circ})$ the same as the pristine GnP, indicating that EGO has a similar interlayer spacing of 0.337 nm as in pristine graphene. This indicates that the functionalization scheme based on Miao's approach²⁰ mostly accessed the edge of graphene without penetrating the

interlayer spacing. The XRD pattern for EGO also exhibits a very weak peak at $2\theta=13.5^{\circ},^{56}$ this corresponds to the introduction of oxygen groups at the edge of graphene. This localization of functional groups on graphene edges for EGO leaves the basal plane mostly intact, preserving the high thermal conductivity of graphene.

For graphene oxidized by the Hummers method (BGO), it is observed that the reflection peak at $2\theta=26.5^{\circ}$ completely disappears and shifts to 12.33° indicating a higher interlayer spacing of 0.717 nm; this higher spacing is due to the intercalation of oxygen functional groups in between graphene layers in the GnPs, suggesting oxidation of the basal plane of all graphene sheets within the GnPs for BGO, resulting in a disordered graphitic structure. Structure of Struc

3.5. Chemical Group Analysis through FTIR Analysis. FTIR analysis was carried out in attenuated total reflectance (ATR) mode to observe the difference in functional groups for EGO and BGO. Oxidation of graphene leads to the presence of epoxy(C-O-C) and hydroxyl (C-OH) functional groups on the basal plane and carbonyl (C=O) and carboxyl (-COOH) functional groups on the edge according to the Lerf-Klinowski model⁵⁸ (see Figure 1e). Figure 6c shows that EGO exhibits an intense peak at \sim 1740 cm⁻¹⁵⁷ and a peak at \sim 1380 cm⁻¹, ⁵⁹ corresponding to stretching vibrations of (C= O) and (C-O), confirming the presence of carboxyl (-COOH) groups. BGO shows a sharp and intense peak for the epoxy group (C-O-C) at ~ 1231 cm⁻¹, ³⁹ comparatively broader peak for the hydroxyl (-OH) group at ~3400 cm⁻¹,60 which is quite dissimilar from EGO. Outlined FTIR analysis reveals the difference in functional groups present in EGO and BGO. Carboxyl group formation is strongly noticeable in EGO confirming the introduction of an excess of carboxyl groups through the Miao's oxidation scheme (involving the use of sodium chlorate and hydrogen peroxide).

3.6. Thermogravimetric Analysis. Functionalization behavior is also observed with TGA analysis in Figure 6d. Pristine GnP exhibits a minor weight change with temperature indicating the presence of a very small quantity of functional groups. Lower total weight loss for EGO (15 wt %) compared to BGO (~45%) represents smaller quantities of functional groups present in EGO compared to BGO. Weight loss in EGO is found to occur very slowly up to 800 °C, indicating removal of highly stable oxygen groups, which are usually edge functional groups. Quick degradation in BGO in the 110 to 300 °C temperature range is not observed in EGO, which implies that BGO possesses a higher amount of less-stable epoxy and hydroxyl groups in comparison to EGO. 28

3.7. XPS Analysis. XPS analysis (seen in Figure 7) is further used to investigate the differences in oxidation in EGO and BGO samples. Figure 7a shows the presence of a C 1s peak around 285 eV for pristine GnP, and strong peaks of O 1s around 533 eV for EGO and BGO.³⁹ The intensity of the oxygen peak in BGO is higher than that in EGO, suggesting a higher atomic percentage of oxygen functional groups in BGO compared to EGO (Figure 7b). The O/C ratios for EGO and BGO are 0.24 and 0.41, respectively.

To understand the differences in functional groups in EGO and BGO, the C 1s high resolution XPS spectra were further analyzed. The deconvoluted spectra of BGO (shown in Figure 7d) reveal the presence of non-oxygenated peaks of C-C/C=C at 284.84 eV, C-O-C (epoxy) at 287.14 eV, C-OH

(hydroxyl) at 286.07 eV, C=O (carbonyl) at 288.83 eV, and O=C-OH (carboxyl) at 290.82 eV. 62,63 Table 1 reveals that

Table 1. Concentration of Functional Groups of EGO and BGO in Atomic Percentage

	C-C/C=C	С-ОН	C-O-C	c=o	О=С-ОН
EGO	62.99		26.87		10.14
BGO	46.28	8.49	33.48	10.25	1.51

the atomic percentage of epoxy and hydroxyl functional groups (as shown in Table 1) in BGO is higher than that in EGO. These functional groups penetrate the graphitic structure modifying the basal plane of BGO, as indicated by the weaker intensity of C-C/C=C in BGO relative to EGO. Such a modification of the basal plane in BGO lowers the thermal conductivity of BGO relative to pristine GnP.

Contrary to the case of BGO, Figure 7c shows that EGO exhibits a significant presence of carboxyl groups, which are known to be predominantly located at the edges of graphene. This combined with the presence of a smaller quantity of epoxy groups (C–O–C peak at 286.78 eV^{63,64}) and the absence of hydroxyl groups (C–OH) in EGO preserve the structural integrity of the basal plane of graphene in EGO. The stronger intensity of the C–C/C=C peak in EGO (Table 1) further confirms the superior integrity of graphene in EGO through the controlled edge oxidation scheme used in this work. The minimal distortion of the basal plane of graphene in EGO preserves its high intrinsic thermal conductivity.

4. CONCLUSIONS

In summary, we have demonstrated the superiority of edge oxidized graphene (EGO) in enhancing the thermal conductivity of graphene/polyetherimide (PEI) composite, relative to basal-plane oxidized graphene (BGO). To achieve edge oxidation, graphene was oxidized with sodium chlorate and hydrogen peroxide in sulfuric acid, introducing an excess of carboxyl groups on graphene edges. Basal plane oxidation was achieved using the Hummers method. The combined effects of the preservation of high intrinsic thermal conductivity of graphene and an enhancement in interfacial thermal conductance between polyetherimide and graphene through edge oxidation caused the thermal conductivity of the EGO/PEI composite to exceed that of the pristine graphene/ PEI composite by almost 18% at 10 wt % graphene composition. Oxidation of the basal plane, however, dramatically lowers the intrinsic thermal conductivity of graphene, causing the k value of the BGO/PEI composite to be diminished by 57 and 63% relative to those of pristine graphene/PEI and EGO/PEI composites, respectively, at the same composition. EGO was found to enhance composite *k* by 725% at 15 wt % composition, while the corresponding enhancement through basal plane oxidation was only ~75% relative to pure PEI. Raman spectroscopy, XPS analysis, XRD, and FTIR analysis provided evidence for the preferential edge oxidation in EGO through the presence of an excess of carboxyl (-COOH) functional groups on graphene edges. These results open up new avenues to achieve higher thermal conductivity polymer-graphene nanocomposites, with important implications for a wide range of thermal management technologies.

Measurement of Through-Thickness Thermal Conductivity. Thermal conductivity measurements were per-

formed though the laser flash technique. A Netzsch LFA 467 Hyperflash laser was used to measure the through-thickness thermal diffusivity of the samples. A short, pulsed laser beam is impinged on one side of the sample, and the temperature is measured on the opposing side of the sample as a function of time. The film samples were cut into circles with a 12.5 mm diameter and coated with a thin layer of graphite paint to increase the emissivity of the samples. Measurements were performed at room temperature (23 $^{\circ}\text{C}$) and a total of 6–8 shots per sample were taken for each sample. The thermal diffusivity was determined using the following equation

$$\alpha = (0.1388d^2)/t_{1/2} \tag{2}$$

where, α is the thermal diffusivity, $t_{1/2}$ is the time to obtain half of the maximum temperature on the rear surface, and d denotes the sample thickness. The thermal conductivity was calculated based on the following equation

$$k = \alpha \rho C_{\rm p} \tag{3}$$

where k, ρ , and $C_{\rm p}$ represent the thermal conductivity, density, and specific heat of the sample, respectively. In this work, density and specific heat of the sample are calculated from the rule of mixtures.

Molecular Structure Characterization. A DXR3 Raman microscope from Thermo Fisher Scientific was used to collect the Raman spectra (shown in Figure 5). The following parameters were used to collect the spectra—a laser wavelength λL of 532 nm, a laser power at the sample of 0.5 mW, and a microscope objective of $100\times$. A 25 mm confocal pinhole aperture and 10 s collection for each spectrum were used. The Raman spectra shown in Figure 6a have been obtained using a Horiba Jobin-Yvon labRam HR instrument. Data were collected over the range from 2400 to 1000 cm^{-1} using a laser wavelength λL of 633 nm, a spectral resolution of 0.16 cm⁻¹, and an imaging resolution of 702 nm. An Olympus BX 41 microscope with a $5\times$ objective, an exposure time of 10 s for 15 accumulations, and three scans per sample was used to collect the spectra.

A Rigaku SmartLab 3kW (Rigaku Corporation, Japan) was used to obtain the XRD patterns of GnP, EGO, and BGO at room temperature using Cu K α radiation (λ = 1.5406 Å) with a scan range of 2–8° min⁻¹ and a step size of 0.02°. The Bragg–Brentano configuration was used to collect the data at room temperature, and the operating parameters were applied over 2θ = 5–70°.

GnP, EGO, and BGO were analyzed by Thermo Scientific K-alpha XPS, where an Al $K\alpha$ gun source was used to excite the sample and measurement was carried out for an acquisition time of ~48 s at a spot size of 400 μ m. A passing energy of 50 eV was utilized to find the C, O peak in this analysis spectrum. The elemental composition of C and O as well as the abundance of functional groups were investigated using the Avantage software. To determine the functional groups' peak position, full width at half-maximum (fwhm), and atomic percentage, Avantage software was used to do curve fitting utilizing Gaussian and Lorentzian functions.

The FT-IR spectra were collected on the GnP, EGO, and BGO samples using a Paragon 1000 FT-IR Spectrometer (PerkinElmer, Inc) with a germanium crystal in ATR mode. Data were measured over a wavenumber range of 4000 to 500 $\,\mathrm{cm}^{-1}$, and OMNIC software was used for spectral analysis.

TGA was performed using a NETZSCH TG 209 F1 Libra to evaluate the thermal stability of the graphene samples and functional groups attached during the oxidation process. Data were collected over the temperature range of 50–800 °C. N_2 gas atmosphere was used with a heating rate of 10 °C/min.

Field Emission Environmental Scanning Electron Microscopy was used to characterize the composite structure. A Thermo Fisher Quattro S FE-ESEM system was operated at 20 kV to perform the analysis of the samples. Morphological characterization of pristine GnP, EGO, and BGO was carried out using SEM and HR-TEM (as presented in Figures S2 and S3, respectively). A Zeiss NEON 40 EsB Crossbeam instrument and a JEOL 2000-FX 200kV transmission electron microscope with a camera for acquisition of DE (Direct Electron)-12 were used to perform the high-resolution SEM and TEM analysis, respectively. This field-emitting scanning electron microscope was operated at an accelerating voltage of 5 kV. To prepare the samples for SEM imaging, the DMAc solvent was used to coat the smooth silicon surface, and a 300 mesh lacy carbon copper grid was used for TEM.

ASSOCIATED CONTENT

Solution Supporting Information

The Supporting Information is available free of charge at https://pubs.acs.org/doi/10.1021/acsami.1c25279.

2D Raman mapping procedure; fwhm for D and G bands of GnP, EGO, and BGO; and SEM and TEM images of GnP, EGO, and BGO (PDF)

AUTHOR INFORMATION

Corresponding Author

Jivtesh Garg — School of Aerospace and Mechanical Engineering, University of Oklahoma, Norman, Oklahoma 73019, United States; orcid.org/0000-0001-8436-0537; Email: garg@ou.edu

Authors

Fatema Tarannum — School of Aerospace and Mechanical Engineering, University of Oklahoma, Norman, Oklahoma 73019, United States; orcid.org/0000-0003-2484-1683

Rajmohan Muthaiah — School of Aerospace and Mechanical Engineering, University of Oklahoma, Norman, Oklahoma 73019, United States

Swapneel Danayat — School of Aerospace and Mechanical Engineering, University of Oklahoma, Norman, Oklahoma 73019, United States

Kayla Foley — Department of Chemical Engineering, University of Arkansas, Fayetteville, Arkansas 72701, United States

Roshan S. Annam — School of Aerospace and Mechanical Engineering, University of Oklahoma, Norman, Oklahoma 73019, United States

Keisha B. Walters — Department of Chemical Engineering, University of Arkansas, Fayetteville, Arkansas 72701, United States; orcid.org/0000-0002-0875-2659

Complete contact information is available at: https://pubs.acs.org/10.1021/acsami.1c25279

Notes

The authors declare no competing financial interest.

ACKNOWLEDGMENTS

R.M., F.T., S.D., and J.G. acknowledge support from the National Science Foundation CAREER award under award no. #1847129. We also thank Mohammed Ibrahim, PhD, from Thermo Fisher Scientific for collecting the Raman spectra for 2D composite mapping.

REFERENCES

- (1) Bar-Cohen, A. Thermal management of on-chip hot spots and 3D chip stacks. 2009 IEEE International Conference on Microwaves, Communications, Antennas and Electronics Systems; IEEE, 2009; pp 1—8. Saadah, M. A. Thermal Management of Solar Cells; UC Riverside, 2013.
- (2) Dreiser, C.; Bart, H.-J. Mineral scale control in polymer film heat exchangers. *Appl. Therm. Eng.* **2014**, *65*, 524–529.
- (3) Mallik, S.; Ekere, N.; Best, C.; Bhatti, R. Investigation of thermal management materials for automotive electronic control units. *Appl. Therm. Eng.* **2011**, *31*, 355–362.
- (4) Lee, J.-K.; Lee, Y.-J.; Chae, W.-S.; Sung, Y.-M. Enhanced ionic conductivity in PEO-LiClO 4 hybrid electrolytes by structural modification. *J. Electroceram.* **2006**, *17*, 941–944.
- (5) Huynh, W. U.; Dittmer, J. J.; Alivisatos, A. P. Hybrid nanorod-polymer solar cells. *Science* **2002**, 295, 2425–2427.
- (6) Luo, B.; Liu, S.; Zhi, L. Chemical approaches toward graphene-based nanomaterials and their applications in energy-related areas. *Small* **2012**, *8*, 630–646.
- (7) Lu, X.; Xu, G. Thermally conductive polymer composites for electronic packaging. J. Appl. Polym. Sci. 1997, 65, 2733–2738.
- (8) Naghibi, S.; Kargar, F.; Wright, D.; Huang, C. Y. T.; Mohammadzadeh, A.; Barani, Z.; Salgado, R.; Balandin, A. A. Noncuring graphene thermal interface materials for advanced electronics. *Adv. Electron. Mater.* **2020**, *6*, 1901303.
- (9) Balandin, A. A. Phononics of graphene and related materials. *ACS Nano* **2020**, *14*, 5170–5178.
- (10) Colonna, S.; Battegazzore, D.; Eleuteri, M.; Arrigo, R.; Fina, A. Properties of Graphene-Related Materials Controlling the Thermal Conductivity of Their Polymer Nanocomposites. *Nanomaterials* **2020**, 10, 2167.
- (11) Barani, Z.; Mohammadzadeh, A.; Geremew, A.; Huang, C. Y.; Coleman, D.; Mangolini, L.; Kargar, F.; Balandin, A. A. Thermal properties of the binary-filler hybrid composites with graphene and copper nanoparticles. *Adv. Funct. Mater.* 2020, 30, 1904008. Cui, X.; Ding, P.; Zhuang, N.; Shi, L.; Song, N.; Tang, S. Thermal conductive and mechanical properties of polymeric composites based on solution-exfoliated boron nitride and graphene nanosheets: a morphology-promoted synergistic effect. *ACS Appl. Mater. Interfaces* 2015, 7, 19068–19075.
- (12) Tarannum, F.; Muthaiah, R.; Annam, R. S.; Gu, T.; Garg, J. Effect of Alignment on Enhancement of Thermal Conductivity of Polyethylene–Graphene Nanocomposites and Comparison with Effective Medium Theory. *Nanomaterials* **2020**, *10*, 1291. Yan, H.; Tang, Y.; Long, W.; Li, Y. Enhanced thermal conductivity in polymer composites with aligned graphene nanosheets. *J. Mater. Sci.* **2014**, *49*, 5256–5264.
- (13) Saeidijavash, M.; Garg, J.; Grady, B.; Smith, B.; Li, Z.; Young, R. J.; Tarannum, F.; Bekri, N. B. High thermal conductivity through simultaneously aligned polyethylene lamellae and graphene nanoplatelets. *Nanoscale* **2017**, *9*, 12867–12873.
- (14) Shahil, K. M. F.; Balandin, A. A. Graphene-multilayer graphene nanocomposites as highly efficient thermal interface materials. *Nano Lett.* **2012**, *12*, 861–867.
- (15) Xu, Y.; Wang, X.; Hao, Q. A mini review on thermally conductive polymers and polymer-based composites. *Compos. Commun.* **2021**, *24*, 100617.
- (16) Lin, S.; Buehler, M. J. The effect of non-covalent functionalization on the thermal conductance of graphene/organic interfaces. *Nanotechnology* **2013**, *24*, 165702.

- (17) Georgakilas, V.; Otyepka, M.; Bourlinos, A. B.; Chandra, V.; Kim, N.; Kemp, K. C.; Hobza, P.; Zboril, R.; Kim, K. S. Functionalization of graphene: covalent and non-covalent approaches, derivatives and applications. *Chem. Rev.* **2012**, *112*, 6156–6214.
- (18) Wang, M.; Hu, N.; Zhou, L.; Yan, C. Enhanced interfacial thermal transport across graphene—polymer interfaces by grafting polymer chains. *Carbon* **2015**, *85*, 414–421.
- (19) Shen, X.; Wang, Z.; Wu, Y.; Liu, X.; He, Y.-B.; Kim, J.-K. Multilayer graphene enables higher efficiency in improving thermal conductivities of graphene/epoxy composites. *Nano Lett.* **2016**, *16*, 3585–3593
- (20) Miao, Z.; Li, X.; Zhi, L. Controlled functionalization of graphene with carboxyl moieties toward multiple applications. *RSC Adv.* **2016**, *6*, 58561–58565.
- (21) Hummers, W. S.; Offeman, R. E. Preparation of Graphitic Oxide. J. Am. Chem. Soc. 1958, 80, 1339.
- (22) Wang, M.; Galpaya, D.; Lai, Z. B.; Xu, Y.; Yan, C. Surface functionalization on the thermal conductivity of graphene–polymer nanocomposites. *Int. J. Smart Nano Mater.* **2014**, *5*, 123–132.
- (23) Konatham, D.; Striolo, A. Thermal boundary resistance at the graphene-oil interface. *Appl. Phys. Lett.* **2009**, *95*, 163105.
- (24) Ganguli, S.; Roy, A. K.; Anderson, D. P. Improved thermal conductivity for chemically functionalized exfoliated graphite/epoxy composites. *Carbon* **2008**, *46*, 806–817.
- (25) Teng, C.-C.; Ma, C.-C. M.; Chiou, K.-C.; Lee, T.-M. Thermal conductivity and morphology of non-covalent functionalized graphene/epoxy nanocomposites. 2010 5th International Microsystems Packaging Assembly and Circuits Technology Conference; IEEE, 2010; pp 1–4.
- (26) Yang, H.; Li, J.-S.; Zeng, X. Correlation between molecular structure and interfacial properties of edge or basal plane modified graphene oxide. *ACS Appl. Nano Mater.* **2018**, *1*, 2763–2773.
- (27) Mungse, H. P.; Kumar, N.; Khatri, O. P. Synthesis, dispersion and lubrication potential of basal plane functionalized alkylated graphene nanosheets. *RSC Adv.* **2015**, *5*, 25565–25571.
- (28) Rezvani Moghaddam, A.; Kamkar, M.; Ranjbar, Z.; Sundararaj, U.; Jannesari, A.; Ranjbar, B. Tuning the network structure of graphene/epoxy nanocomposites by controlling edge/basal localization of functional groups. *Ind. Eng. Chem. Res.* **2019**, *58*, 21431–21440.
- (29) Xiang, Z.; Dai, Q.; Chen, J.-F.; Dai, L. Edge functionalization of graphene and two-dimensional covalent organic polymers for energy conversion and storage. *Adv. Mater.* **2016**, *28*, 6253–6261.
- (30) Pei, S.; Cheng, H.-M. The reduction of graphene oxide. *Carbon* **2012**, *50*, 3210–3228. Eigler, S.; Grimm, S.; Enzelberger-Heim, M.; Müller, P.; Hirsch, A. Graphene oxide: efficiency of reducing agents. *Chem. Commun.* **2013**, *49*, 7391–7393.
- (31) Compton, O. C.; Nguyen, S. T. Graphene oxide, highly reduced graphene oxide, and graphene: versatile building blocks for carbon-based materials. *Small* **2010**, *6*, 711–723.
- (32) Bagri, A.; Grantab, R.; Medhekar, N. V.; Shenoy, V. B. Stability and Formation Mechanisms of Carbonyl- and Hydroxyl-Decorated Holes in Graphene Oxide. *J. Phys. Chem. C* **2010**, *114*, 12053–12061.
- (33) Fugallo, G.; Cepellotti, A.; Paulatto, L.; Lazzeri, M.; Marzari, N.; Mauri, F. Thermal conductivity of graphene and graphite: collective excitations and mean free paths. *Nano Lett.* **2014**, *14*, 6109–6114.
- (34) Mu, X.; Wu, X.; Zhang, T.; Go, D. B.; Luo, T. Thermal transport in graphene oxide—from ballistic extreme to amorphous limit. *Sci. Rep.* **2014**, *4*, 3909.
- (35) Shenogin, S.; Bodapati, A.; Xue, L.; Ozisik, R.; Keblinski, P. Effect of chemical functionalization on thermal transport of carbon nanotube composites. *Appl. Phys. Lett.* **2004**, *85*, 2229–2231.
- (36) Wang, G.; Yang, J.; Park, J.; Gou, X.; Wang, B.; Liu, H.; Yao, J. Facile synthesis and characterization of graphene nanosheets. *J. Phys. Chem. C* **2008**, *112*, 8192–8195. Choi, Y. S.; Yeo, C.-s.; Kim, S. J.; Lee, J.-Y.; Kim, Y.; Cho, K. R.; Ju, S.; Hong, B. H.; Park, S. Y. Multifunctional reduced graphene oxide-CVD graphene core—shell fibers. *Nanoscale* **2019**, *11*, 12637–12642.

- (37) Navaee, A.; Salimi, A. Efficient amine functionalization of graphene oxide through the Bucherer reaction: an extraordinary metal-free electrocatalyst for the oxygen reduction reaction. *RSC Adv.* **2015**, *5*, 59874–59880. Hussein, A.; Sarkar, S.; Oh, D.; Lee, K. Epoxy/p-phenylenediamine functionalized graphene oxide composites and evaluation of their fracture toughness and tensile properties. *J. Appl. Polym. Sci.* **2016**, *133*, 43821. DOI: 10.1002/app.43821
- (38) Han, D.; Zhao, Y.-H.; Zhang, Y.-F.; Bai, S.-L. Vertically and compactly rolled-up reduced graphene oxide film/epoxy composites: a two-stage reduction method for graphene-based thermal interfacial materials. *RSC Adv.* **2015**, *5*, 94426–94435.
- (39) Hwang, Y.; Heo, Y.; Yoo, Y.; Kim, J. The addition of functionalized graphene oxide to polyetherimide to improve its thermal conductivity and mechanical properties. *Polym. Adv. Technol.* **2014**, 25, 1155–1162.
- (40) Bernal, M. M.; Di Pierro, A.; Novara, C.; Giorgis, F.; Mortazavi, B.; Saracco, G.; Fina, A. Edge-Grafted Molecular Junctions between Graphene Nanoplatelets: Applied Chemistry to Enhance Heat Transfer in Nanomaterials. *Adv. Funct. Mater.* **2018**, *28*, 1706954.
- (41) Muthaiah, R.; Tarannum, F.; Danayat, S.; Annam, R. S.; Nayal, A. S.; Yedukondalu, N.; Garg, J. Superior effect of edge relative to basal plane functionalization of graphene in enhancing polymergraphene nanocomposite thermal conductivity-A combined molecular dynamics and Greens functions study. 2022, arXiv:2201.01011. arXiv preprint.
- (42) Balandin, A. A. Thermal properties of graphene and nanostructured carbon materials. *Nat. Mater.* **2011**, *10*, 569–581.
- (43) Zhang, W.; Fisher, T. S.; Mingo, N. The Atomistic Green's Function Method: An Efficient Simulation Approach for Nanoscale Phonon Transport. *Numer. Heat Transfer, Part B* **2007**, *51*, 333–349.
- (44) Yuge, R.; Zhang, M.; Tomonari, M.; Yoshitake, T.; Iijima, S.; Yudasaka, M. Site identification of carboxyl groups on graphene edges with Pt derivatives. *ACS Nano* **2008**, *2*, 1865–1870.
- (45) Radovic, L. R.; Mora-Vilches, C. V.; Salgado-Casanova, A. J. A.; Buljan, A. Graphene functionalization: Mechanism of carboxyl group formation. *Carbon* **2018**, *130*, 340–349.
- (46) Graphene Supermarket. https://graphene-supermarket.com/Graphene-Nanopowder-AO-4-60-nm-Flakes-25-g.html (accessed 2020-08-09).
- (47) MilliporeSigma. https://www.sigmaaldrich.com/US/en/product/aldrich/700207/ (accessed 2020-08-09).
- (48) Wu, H.; Drzal, L. T. High thermally conductive graphite nanoplatelet/polyetherimide composite by precoating: Effect of percolation and particle size. *Polym. Compos.* **2013**, *34*, 2148–2153.
- (49) Marcano, D. C.; Kosynkin, D. V.; Berlin, J. M.; Sinitskii, A.; Sun, Z.; Slesarev, A.; Alemany, L. B.; Lu, W.; Tour, J. M. Improved synthesis of graphene oxide. *ACS Nano* **2010**, *4*, 4806–4814. Yadav, N.; Lochab, B. A comparative study of graphene oxide: Hummers, intermediate and improved method. *FlatChem* **2019**, *13*, 40–49. Botas, C.; Álvarez, P.; Blanco, C.; Santamaría, R.; Granda, M.; Ares, P.; Rodríguez-Reinoso, F.; Menéndez, R. The effect of the parent graphite on the structure of graphene oxide. *Carbon* **2012**, *50*, 275–282.
- (50) Bepete, G.; Pénicaud, A.; Drummond, C.; Anglaret, E. Raman Signatures of Single Layer Graphene Dispersed in Degassed Water, "Eau de Graphene". *J. Phys. Chem. C* **2016**, *120*, 28204–28214.
- (51) Ganguly, A.; Sharma, S.; Papakonstantinou, P.; Hamilton, J. Probing the thermal deoxygenation of graphene oxide using high-resolution in situ X-ray-based spectroscopies. *J. Phys. Chem. C* **2011**, 115, 17009–17019.
- (52) Chen, Q.; Yan, X.; Wu, L.; Xiao, Y.; Wang, S.; Cheng, G.; Zheng, R.; Hao, Q. Small-Nanostructure-Size-Limited Phonon Transport within Composite Films Made of Single-Wall Carbon Nanotubes and Reduced Graphene Oxides. *ACS Appl. Mater. Interfaces* **2021**, *13*, 5435–5444.
- (53) Cao, H.; Wu, X.; Yin, G.; Warner, J. H. Synthesis of adenine-modified reduced graphene oxide nanosheets. *Inorg. Chem.* **2012**, *51*, 2954–2960.

- (54) Li, J.; Zeng, X.; Ren, T.; Van der Heide, E. The preparation of graphene oxide and its derivatives and their application in biotribological systems. *Lubricants* **2014**, *2*, 137–161.
- (55) Chhabra, V.; Deep, A.; Kaur, R.; Kumar, R. Functionalization of graphene using carboxylation process. *Int. J. Sci. Emerg. Technol.* **2012**, 4, 13–19.
- (56) Krishnamoorthy, K.; Veerapandian, M.; Yun, K.; Kim, S.-J. The chemical and structural analysis of graphene oxide with different degrees of oxidation. *Carbon* **2013**, *53*, 38–49.
- (57) Shahriary, L.; Athawale, A. A. Graphene oxide synthesized by using modified hummers approach. *Int. J. Renew. Energy Environ. Eng.* **2014**, 2, 58–63.
- (58) Lerf, A.; He, H.; Forster, M.; Klinowski, J. Structure of graphite oxide revisited. *J. Phys. Chem. B* **1998**, 102, 4477–4482.
- (59) Tabish, T.; Pranjol, M.; Horsell, D.; Rahat, A.; Whatmore, J.; Winyard, P.; Zhang, S. Graphene oxide-based targeting of extracellular cathepsin D and cathepsin L as a novel anti-metastatic enzyme cancer therapy. *Cancers* **2019**, *11*, 319.
- (60) Park, J.; Kim, Y. S.; Sung, S. J.; Kim, T.; Park, C. R. Highly dispersible edge-selectively oxidized graphene with improved electrical performance. *Nanoscale* **2017**, *9*, 1699–1708.
- (61) Hack, R.; Correia, C. H. G.; Zanon, R. A. d. S.; Pezzin, S. H. Characterization of graphene nanosheets obtained by a modified Hummer's method. *Matéria* **2018**, 23, No. e-11988.
- (62) Aliyev, E.; Filiz, V.; Khan, M. M.; Lee, Y. J.; Abetz, C.; Abetz, V. Structural characterization of graphene oxide: Surface functional groups and fractionated oxidative debris. *Nanomaterials* **2019**, *9*, 1180.
- (63) Stobinski, L.; Lesiak, B.; Malolepszy, A.; Mazurkiewicz, M.; Mierzwa, B.; Zemek, J.; Jiricek, P.; Bieloshapka, I. Graphene oxide and reduced graphene oxide studied by the XRD, TEM and electron spectroscopy methods. *J. Electron Spectrosc. Relat. Phenom.* **2014**, 195, 145–154.
- (64) Drewniak, S.; Muzyka, R.; Stolarczyk, A.; Pustelny, T.; Kotyczka-Morańska, M.; Setkiewicz, M. Studies of reduced graphene oxide and graphite oxide in the aspect of their possible application in gas sensors. *Sensors* **2016**, *16*, 103.